AIP Applied Physics Letters

Micro-textured conductive polymer/silicon heterojunction photovoltaic devices with high efficiency

Ting-Gang Chen, Bo-Yu Huang, En-Chen Chen, Peichen Yu, and Hsin-Fei Meng

Citation: Applied Physics Letters **101**, 033301 (2012); doi: 10.1063/1.4734240
View online: http://dx.doi.org/10.1063/1.4734240
View Table of Contents: http://scitation.aip.org/content/aip/journal/apl/101/3?ver=pdfcov
Published by the AIP Publishing

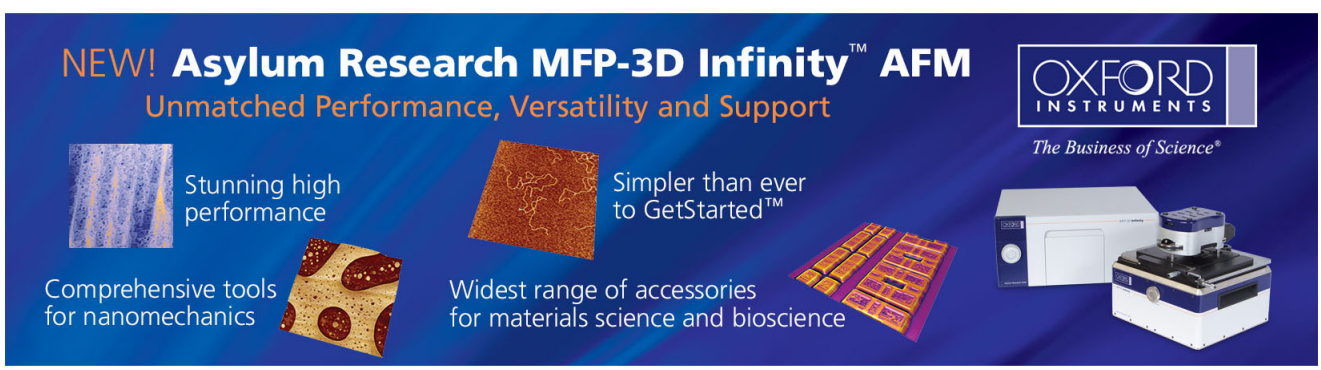

Micro-textured conductive polymer/silicon heterojunction photovoltaic devices with high efficiency

Ting-Gang Chen,[1] Bo-Yu Huang,[1] En-Chen Chen,[2] Peichen Yu,[1,a)] and Hsin-Fei Meng[2,b)]
[1]*Department of Photonics and Institute of Electro-Optical Engineering, National Chiao Tung University, Hsinchu 30010, Taiwan*
[2]*Institute of Physics, National Chiao Tung University, Hsinchu 30010, Taiwan*

(Received 9 January 2012; accepted 22 May 2012; published online 16 July 2012)

In this work, hybrid heterojunction solar cells are demonstrated based on a conjugate polymer poly(3,4-ethylenedioxy-thiophene):poly(styrenesulfonate) (PEDOT:PSS) directly spun-cast on micro-textured n-type crystalline silicon wafers. The fabrication conditions suggest that the organic coverage on the micro-textured surface is excellent and key to achieve high efficiency, leading to an average power conversion efficiency of 9.84%. A one-dimensional drift-diffusion model is then developed based on fitting the device characteristics with experimentally determined PEDOT:PSS parameters and projects an ultimate efficiency above 20% for organic/inorganic hybrid photovoltaics. The simulation results reveal the impacts of defect densities, back surface recombination, doping concentration, and band alignment. © *2012 American Institute of Physics*. [http://dx.doi.org/10.1063/1.4734240]

In recent years, photovoltaics have become a most pursued renewable energy technology due to rising concerns about petroleum extinction and greenhouse effects. Currently, mono- and multi-crystalline silicon photovoltaics still hold more than 80% market share because of the non-toxic, abundant material resources used, and their long-term stabilities.[1] However, the cost of solar power is still more than three times that of fossil fuels, which necessitates a further reduction to accelerate its widespread use. It has been estimated that cell fabrication consumes 30% of the total manufacturing cost due to energy intensive semiconductor processes, such as high temperature furnace for doping, electrodes co-firing, high-vacuum chemical deposition, etc.[2,3] Therefore, the organic-inorganic hybrid cell concept has been proposed to take advantage of the solution-based processes for rapid and low-cost production and the wide absorption spectrum of silicon.[4–6] Over the past few years, hybrid devices based on the composites of conjugated polymer/silicon heterojunction structures, such as poly (3-hexylthiophene) (P3HT)/Si and poly(3,4-ethylenedioxy-thiophene):poly(styrenesulfonate) (PEDOT:PSS)/Si, have advanced steadily.[7–9] The recent incorporation of silicon nanowire arrays pushes the power conversion efficiency (PCE) to around 10%, mainly attributed to the suppressed front surface reflection and the increased junction area by forming a core-shell structure.[10–12] However, SiNW arrays add complexity to the device design and fabrication due to trade-offs between light management and surface recombination, as well as control of the length uniformity in whole wafers. In this work, we demonstrate hybrid heterojunction solar cells based on the composite conductive polymer PEDOT:PSS directly spun-cast on a micro-textured, n-type crystalline silicon wafer rather than nanowire structures. The optimized random pyramids permit low reflectance without introducing severe surface recombination, which is crucial to photovoltaic devices. Moreover, the fabrication conditions suggest that the organic coverage on the micro-textured surface is excellent and key to achieve high efficiency. The simple solution-based fabrication process results in an average PCE of 9.84%, which is among the highest values for hybrid devices.[10–12] We further develop a device modeling technique for organic/inorganic heterojunction devices, which projects an ultimate PCE above 20%. The simulation results reveal the impacts of defect densities, back surface recombination, doping concentration, and band alignment on the device performance.

The hybrid heterojunction solar cells employed an n-type solar-grade mono-crystalline silicon substrate with a thickness of 200 μm and a resistivity of 2 Ω-cm. The micro-textured surfaces were provided by anisotropic wet-etching in aqueous alkaline solutions, forming random pyramids with heights of 2–6 μm. The textured and planar reference samples were subsequently processed into hybrid solar cells. First, the samples were dipped in dilute hydrofluoric acid for 20 s to remove the native oxide and attain a hydrophobic surface, followed by the thermal evaporation of a 100-nm-thick aluminum layer as the back electrode in the glove box. A highly conductive aqueous PEDOS:PSS dispersion (Clevios PH1000) was employed with 5 wt. % dimethyl sulfoxide as a secondary dopant to increase the conductivity. Meanwhile, 0.2 wt. % hexaethylene glycol monododecyl ether was added as a surfactant to improve the adhesion between PEDOT:PSS and silicon. The PEDOT:PSS with additives was spun-cast onto a silicon surface at various speeds for 120 s and heated to 115 °C for 10 min in ambient. Finally, a 100-nm-thick silver frontal electrode was thermally evaporated through a shadow mask. Figures 1(a)–1(d) show the scanning electron micrographs (SEM) of the PEDOT:PSS morphology coated on the pyramidal surfaces at the spin rates of 1000, 4000, 6000, and 8000 rpm, respectively, where the PEDOT:PSS layer is colored in teal for eye guide. The layer thicknesses are roughly equal; however, the coverage is much improved at a high spinning speed. A conformal coverage down to the

a)Electronic mail: yup@faculty.nctu.edu.tw.
b)Electronic mail: meng@mail.nctu.edu.tw.

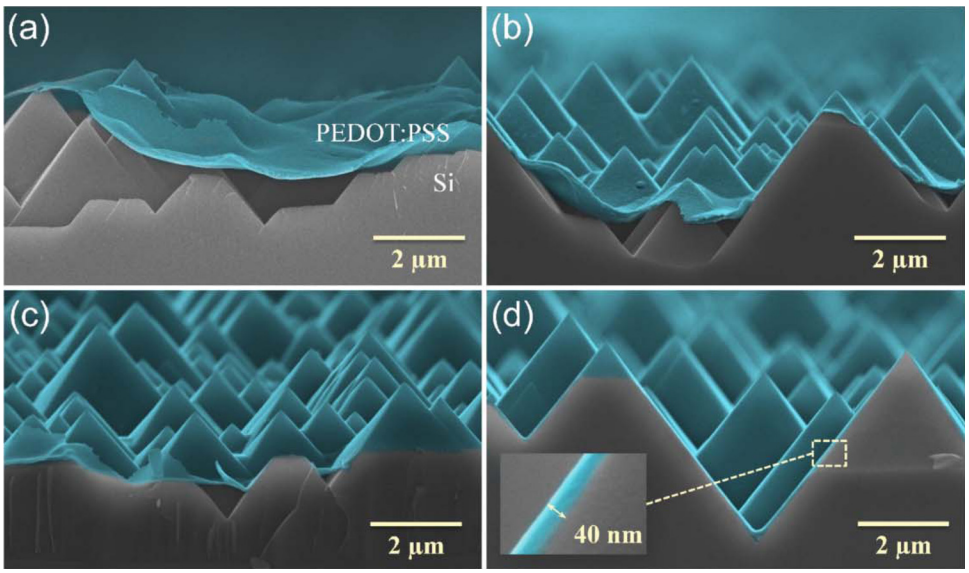

FIG. 1. SEM of (a) PEDOT:PSS/Si solar cells with spin rates of 1000, (b) 4000, (c) 6000, and (d) 8000 rpm, respectively. The PEDOT:PSS thin film is colored in teal for eye guide. The polymer film spun-cast at 8000 rpm shows an excellent coverage onto the pyramidal surface. The inset shows the PEDOT:PSS layer with a tapered thickness of approximately 40 nm in the middle.

valleys is achieved at 8000 rpm. We further measure the film thickness on the pinnacle of pyramids which is ~20 nm and ~60 nm at valleys, leading to an average of 40 nm, as shown in the inset of Fig. 1(d).

The device current density-voltage characteristics were determined using a class A solar simulator with a calibrated illumination intensity of 1000 W/m^2 for the air mass 1.5 global (AM1.5G) solar spectrum, as shown in Fig. 2(a). The open-circuit voltage (V_{oc}), short-circuit current density (J_{sc}), fill-factor (FF), and PCE of fabricated devices are summarized in Table I, which are obtained by averaging three devices with a calculated 95% confident interval. It can be seen in Table I that the V_{oc}, J_{sc}, FF, and PCE of micro-textured hybrid cells are positively correlated with the spin rates. At low spin rates, a large portion of air voids is created between the PEDOT:PSS layer and silicon interface, resulting in a poor contact of heterojunctions. Higher spin rates lead to a better coverage, which facilitates the carrier separation and transport through the PEDOT:PSS layer. The hybrid cells achieve an average PCE of 9.84% at 8000 rpm, which is attributed to the excellent organic coverage on the micro-scale pyramidal surface. In contrast, the planar hybrid cells exhibit a low shutting loss due to the absence of the coverage issue, resulting in a comparable average V_{oc} of 0.5 V. However, the J_{sc} is hindered by the high reflection from planar Si surfaces (see supplementary material),[23] and the FF is impeded by the finite junction area leading to insufficient charge transport pathways, which increases the series resistance. Figure 2(b) shows the measured external quantum efficiency (EQE) and optical reflectance spectra (R) of a micro-textured device with the highest efficiency. The internal quantum efficiency (IQE) which describes the wavelength dependence of charge collection characteristics is also calculated using IQE = EQE/(1−R) for devices with a back reflector and/or thick substrate. As shown in Fig. 2(b), the micro-textured surface exhibits a weighted reflectance of ~9.5% due to multiple surface reflections. Such a value is typical without introducing an antireflective coating, hence limiting the photocurrent output at 30.5 mA/cm^2. Since the spin-coated PEDOT:PSS layer has a low refractive index and very thin thickness, an optically optimized film thickness can hinder the carrier transport. Therefore, advanced antireflection techniques involving nanoscale texturing may still be mandatory to further improve the J_{sc} of micro-textured hybrid solar cells. However, as shown in Fig. 2(b), the IQE is over 95% in the short wavelength range, which is much superior to commercial silicon solar cells due to the wide bandgap of PEDOT:PSS that blocks electrons from being recombined at the front surface. On the other hand, the low IQE in the long wavelength range indicates severe back

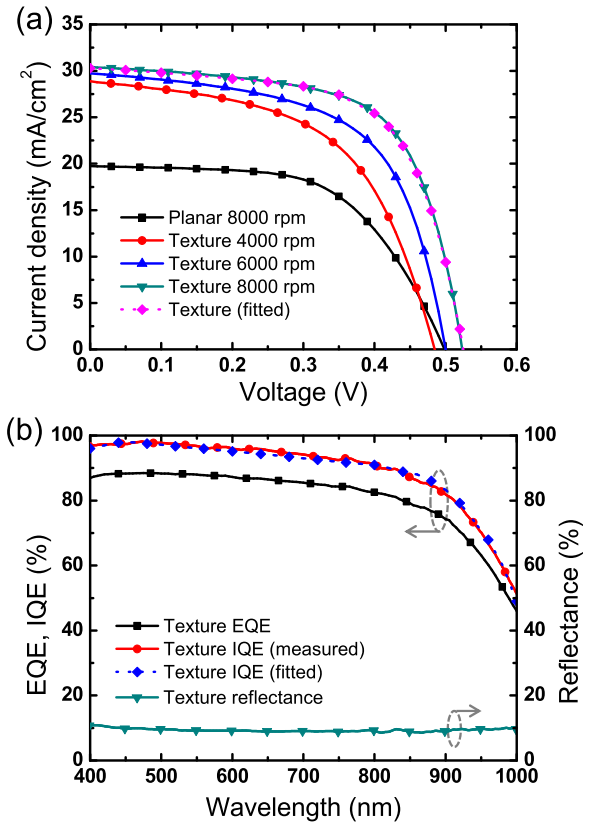

FIG. 2. (a) Measured and calculated current density-voltage characteristics of the micro-textured and planar hybrid cells under a simulated one-sun AM1.5G illumination. (b) Measured EQE and reflectance spectra and the extracted IQE spectrum of a micro-textured hybrid cell fabricated with 8000 rpm. The dotted line indicates a fitted IQE curve.

TABLE I. Averaged photovoltaic characteristics of micro-textured hybrid solar cells fabricated with various spin rates and the planar reference cells with 8000 rpm.

Spin rates	V_{oc} (V)	J_{sc} (mA/cm^2)	FF (%)	PCE[a] (%)
1000 rpm	0.31	21.82	39.74	2.69 ± 0.16
4000 rpm	0.48	28.41	54.59	7.44 ± 0.43
6000 rpm	0.50	29.59	58.73	8.61 ± 0.37
8000 rpm	0.52	30.50	62.13	9.84 ± 0.44
Planar	0.50	19.7	56.6	5.52 ± 0.32

[a]The statistics present the error range of three measured samples with a 95% confident interval.

surface recombination, which requires further improvements to increase J_{sc}.

To better understand the correlation between charge transport and material properties, an electronic model is developed based on a self-consistent solver of one-dimensional (1D) Poisson and continuity equations.[13,14] The program computes the electrostatic potential and quasi-Fermi levels from which the carrier concentrations, fields, and currents can be calculated. Here, the PEDOT:PSS layer is treated as an inorganic semiconductor where the position of the lowest unoccupied molecular orbital and the highest occupied molecular orbital (HOMO) is taken as that of the conduction band and the valence band, respectively. Therefore, the hopping mechanism can be described by the drift-diffusion model as charge transport in a two-terminal solid-state device under dark or illuminated conditions. Since the layer thickness of PEDOT:PSS involved in this device is very thin and the exciton binding energy is lower than other active organic materials, the electronic model allows for full investigation of mechanisms that depict V_{oc} and FF of a hybrid solar cell without making empirical assumptions commonly used in organic solar cells.[15–17] Furthermore, since a 1D model is adequate to describe the charge transport in a micro-textured heterojunction device, the distribution of the carrier generation rate obtained via optical absorption should still be best modeled by the weighted AM1.5G solar spectrum and the measured reflectance using an integrating sphere to fully take into account the scattered optical loss elements. To determine other simulation parameters, the conductivity of a PEDOT:PSS film spun-cast on a glass substrate at 8000 rpm was derived from the film thickness and measured sheet resistance using a four-point-probe method, resulting in a value of 69.4 S/cm. Also, the positions of the work function and ionization energy of the PEDOT:PSS thin film turned out to be 4.75 eV and 5.17 eV, respectively, using ultraviolet photoelectron spectroscopy. Therefore, several fitting parameters including the doping concentration, mobility, bandgap were adjusted to be consistent with the

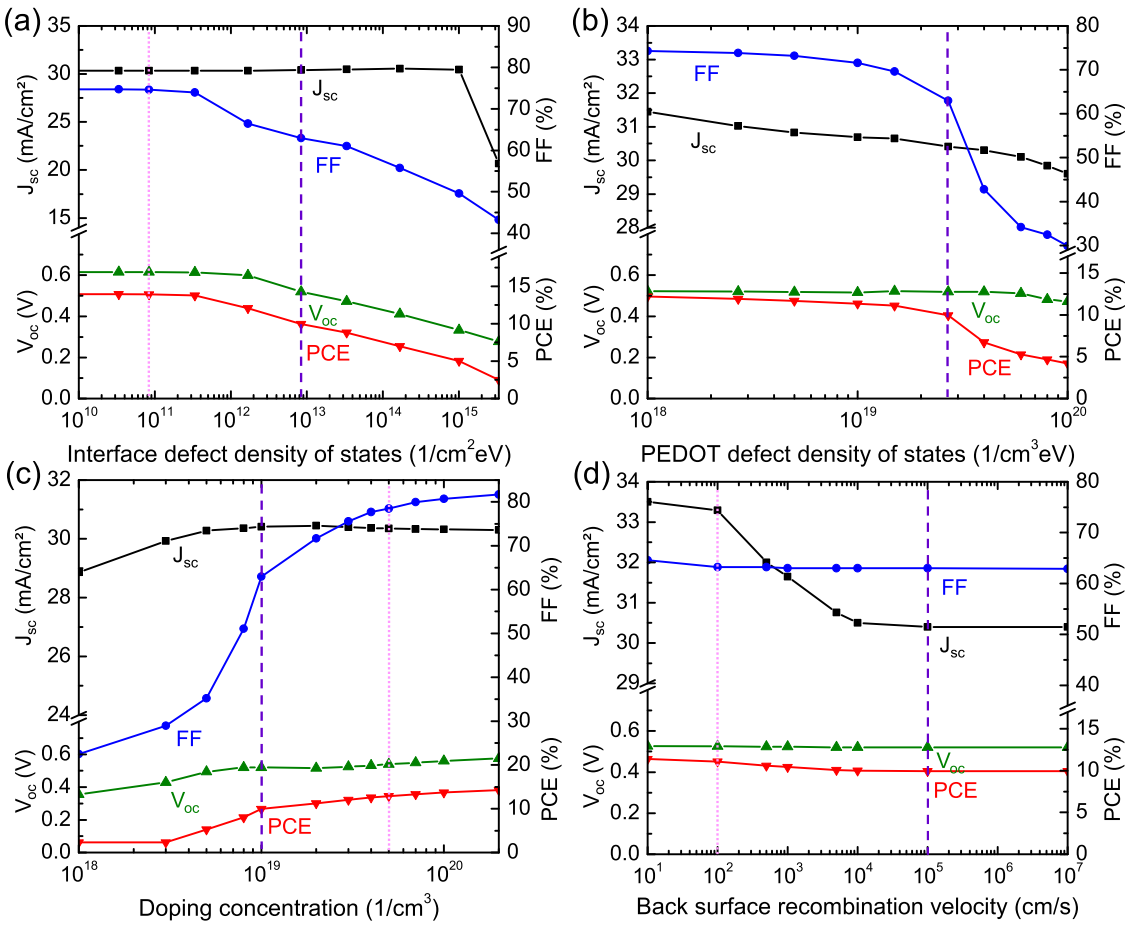

FIG. 3. The calculated photovoltaic characteristics of hybrid solar cells as a function of (a) the interface defect density of states, (b) bulk defect density of states in PEDOT:PSS, (c) doping concentration, and (d) the back surface recombination velocity based on the fitted device model shown in Fig. 2. The purple and pink lines represent the simulation baseline for the fabricated device and for cells with improved material properties to study the effect of band alignments, respectively.

experimental values. The proposed model is then fitted to the measured J-V and IQE curves, as respectively shown in Figs. 2(a) and 2(b) for validation. Detailed parameters are provided in the supplementary material.

To summarize the analyses, we have identified the interface and PEDOT defect density of states, the doping concentration, and the back surface recombination velocity exhibiting strong influence on the photovoltaic characteristics, as depicted in Figs. 3(a)–3(d), respectively. The purple dashed line in Fig. 3 indicates the fitting baseline with the fabricated device characteristics. It can be seen that V_{oc} mainly depends on the interface defect density of states, which is estimated to be $8.4 \times 10^{12}\,cm^{-2}\,eV^{-1}$ for the fabricated device. The interface condition may be further improved by using methyl groups or other organic molecules to passivate dangling bonds or modify surface dipoles before the cast of PEDOT:PSS.[7,18,19] On the other hand, the FF is determined by both the recombination and transport mechanisms. Therefore, as shown in Figs. 3(a)–3(c), reducing the interface and PEDOT:PSS defect densities and increasing the doping concentration of the PEDOT:PSS layer can facilitate the charge transport, which increases the FF. It is important to note that the simulation does not take into account the Auger recombination due to the lack of experimental information, which may slightly limit the FF enhancement at high doping concentrations. Finally, the J_{sc} of the fabricated device is primarily limited by the reflection and metal shadow loss and, therefore, not very sensitive to the interface and bulk defects. However, the IQE characteristics shown in Fig. 2(b) indicate a considerable amount of long-wavelength photogenerated carriers lost to the back surface recombination. Consequently, as shown in Fig. 3(d), reducing the back surface recombination velocity down to 100 cm/s (pink dotted line) can effectively increase the J_{sc} by 3 mA/cm^2, which translates to a nearly 10% improvement in the PCE. Such a low velocity is mandatory for crystalline silicon solar cells with efficiencies over 20% and can be realized by introducing a back surface field to block minority carriers or using various passivation techniques.[20] According to Fig. 3, if the interface and silicon back surface conditions, as well as the doping concentration of PEDOT:PSS are further improved to the values indicated by the pink dotted line, a projected PCE as high as 18.2% can be achieved for the hybrid PEDOT:PSS/Si structure. Since the reflection and metal shadow losses are still quite high for the presented device, it is attainable to control the total loss to be within 10% when the top material has a high conductivity. The efficiency of such devices can be further pushed to be over 20%, as indicated by the yellow symbol shown in Fig. 4(a).

In recent years, there have been several reports on conjugate polymers or small molecule materials with high carrier concentrations and mobilities.[21,22] It is, therefore, informative to investigate the band alignment of these emerging materials with n-type silicon for applications of

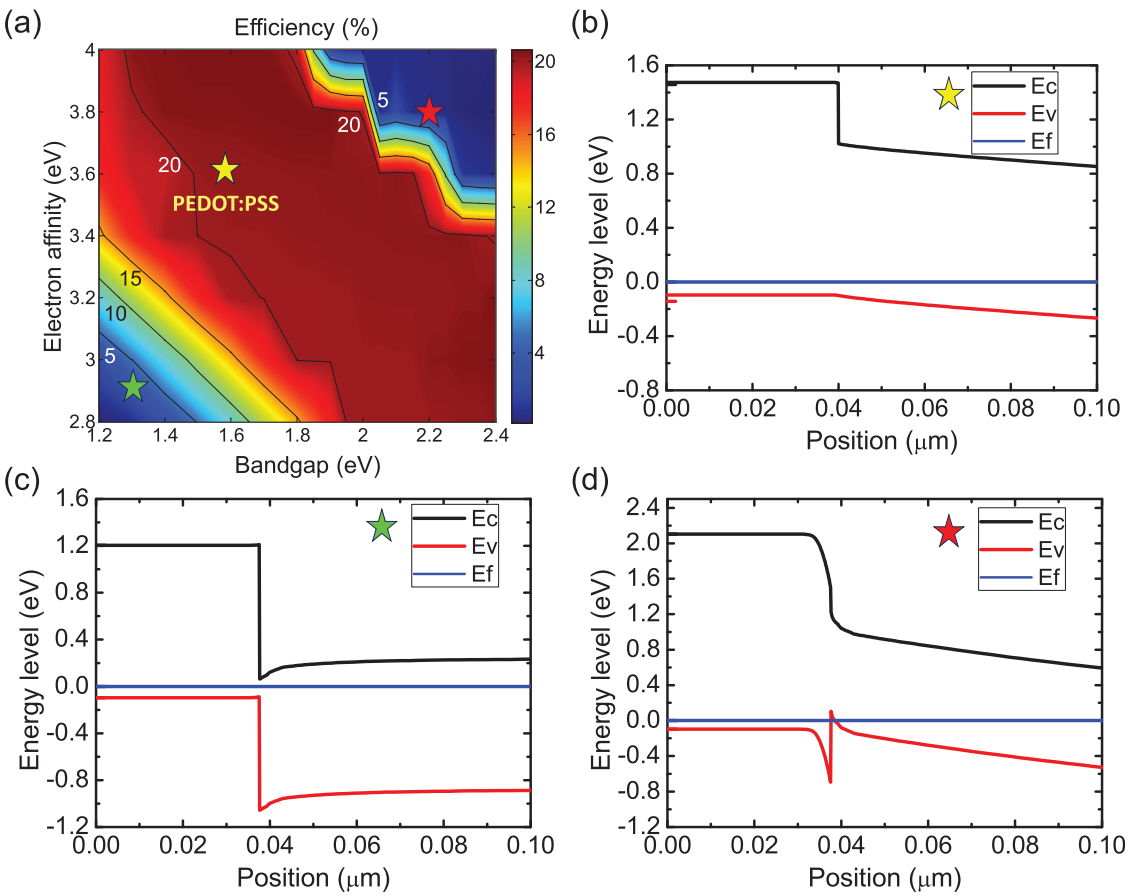

FIG. 4. (a) Efficiency map of hybrid organic/n-Si solar cells as a function of the electron affinity and bandgap. The yellow symbol denotes the properties of PEDOT:PSS, which indicates a projected power conversion efficiency over 20%. (b)–(d) The corresponding band alignment for locations marked by yellow, green, and red star-symbols in the efficiency map, respectively.

hybrid photovoltaics. Figure 4(a) plots a projected efficiency map as a function of electron affinity and energy bandgap with a controlled metal shadow and reflection loss of 10% and desired material properties indicated by the pink dotted lines in Fig. 3. The yellow star-symbol represents the simulated PEDOT:PSS properties with a bandgap of 1.57 eV and electron affinity of 3.6 eV, which demonstrates a projected PCE of 20.1%. The corresponding band alignment is shown in Fig. 4(b), where a large conduction band offset can block electrons from being lost to the front surface recombination, while a small valence band offset can facilitate the hole transport. Contrarily, the green and red star-symbols in Fig. 4(a) mark two ill-performing devices of which the band alignments are shown in Figs. 4(c) and 4(d), respectively. Since the V_{oc} of a solar cell is essentially limited by the quasi-Fermi level separation depicted by the position of the conduction band of silicon and the valence band, i.e., the HOMO level of the organic material, a cell with the band alignment shown in Fig. 4(c) exhibits a small V_{oc}. Moreover, the band bending at the hetero-junction interface could also lead to electron accumulation and, therefore, is not favorable for charge transport. Similarly, the large valence band offset at the heterojunction interface in Fig. 4(d) impedes the hole transport and therefore limits the J_{sc}, leading to a poor PCE. From these perspectives, the band alignment between PEDOT:PSS and silicon is very suitable for hybrid photovoltaic devices.

In conclusion, a hybrid conductive polymer/silicon heterojunction solar cell is demonstrated with an average power conversion efficiency of 9.84% using rapid solution-based organic processes. The modeling of such devices predicts an efficiency exceeding 20% with improved reflection loss and material properties, shedding light into the attainment of high-efficiency and low-cost photovoltaics based on organic/inorganic hybrid devices.

We thank Professor C. I. Wu at the Department of Electrical Engineering, National Taiwan University for helping on the UPS measurement and Professor B. Q. Sun at the Functional Nano & Soft Materials Laboratory (FUNSOM) at the Soochow University for fruitful discussions. This work is founded by National Science Council in Taiwan under Grant number 100-2628-E-009-020-MY3.

[1]R. F. Service, Science **319**, 718 (2008).
[2]R. G. Little and M. J. Nowlan, Prog. Photovolt. **5**, 309 (1997).
[3]V. M. Fthenakis and H. C. Kim, Sol. Energy **85**, 1609 (2010).
[4]M. J. Sailor, E. J. Ginsburg, C. B. Gorman, A. Kumar, R. H. Grubbs, and N. S. Lewis, Science **249**, 1146 (1990).
[5]A. A. D. T. Adikaari, D. M. N. M. Dissanayake, and S. R. P. Silva, IEEE. J. Sel. Top. Quantum **16**, 1595 (2010).
[6]J. W.P. Hsu and M. T. Lloyd, MRS Bull. **35**, 422 (2010).
[7]F. Zhang, B. Sun, T. Song, X. Zhu, and S. T. Lee, Chem. Mater. **23**, 2084 (2011).
[8]S. C. Shiu, J. J. Chao, S. C. Hung, C. L. Yeh, and C. F. Lin, Chem. Mater. **22**, 3108 (2010).
[9]J. C. Nolasco, R. Cabré, J. Ferré-Borrull, L. F. Marsal, M. Estrada, and J. Pallarès, J. Appl. Phys. **107**, 044505 (2010).
[10]L. He, Rusli, C. Jiang, H. Wang, and D. Lai, IEEE Electron Device Lett. **32**, 1406 (2011).
[11]X. Shen, B. Sun, D. Liu, and S. T. Lee, J. Am. Chem. Soc. **133**, 19408 (2011).
[12]L. He, C. Jiang, Rusli, D. Lai, and H. Wang, Appl. Phys. Lett. **99**, 021104 (2011).
[13]J. Cuiffi, T. Benanti, W. J. Nam, and S. Fonash, Appl. Phys. Lett. **96**, 143307 (2010).
[14]Y. Liu, Y. Sun, and A. Rockett, Sol. Energy Mater. Sol. Cells **98**, 124 (2012).
[15]M. C. Scharber, D. Muhlbacher, M. Koppe, P. Denk, C. Waldauf, J. Heeger, and C. J. Brabec, Adv. Mater. **18**, 789 (2006).
[16]C. Waldauff, P. Schilinsky, J. Hauch, and C. J. Brabec, Thin Solid Films **451**, 503 (2004).
[17]P. W. M. Blom, V. D. Mihailetchi, L. J. A. Koster, and D. E. Markov, Adv. Mater. **19**, 1551 (2007).
[18]C. Goh, S. R. Scully, and M. D. McGehee, J. Appl. Phys. **101**, 114503 (2007).
[19]S. Avasthi, Y. Qi, G. K. Vertelov, J. Schwartz, A. Kahn, and J. C. Sturm, Appl. Phys. Lett. **96**, 222109 (2010).
[20]A. Das, V. Meemongkolkiat, D. S. Kim, S. Ramanathan, and A. Rohatgi, IEEE Trans. Electron Devices **57**, 2462 (2010).
[21]J. Y. Kim, M. H. Kwon, Y. K. Min, S. Kwon, and D. W. Ihm, Adv. Mater. **19**, 3501 (2007).
[22]I. Ding, N. Tétreault, J. Brillet, B. E. Hardin, E. H. Smith, S. J. Rosenthal, F. Sauvage, M. Grätzel, and M. D. McGehee, Adv. Funct. Mater. **19**, 2431 (2009).
[23]See supplementary material at http://dx.doi.org/10.1063/1.4734240 for the methodology and results of optical modeling, simulation parameters, and the UPS spectrum of PEDOT:PSS.